Crystal structure of wild-type and mutant human Ap$_4$A hydrolase

Honghua Ge [a],[*],[1], Xiaofang Chen [a],[1], Weili Yang [b], Liwen Niu [a],[b], Maikun Teng [b],[*]

[a] Institute of Health Sciences and Modern Experiment Technology Center, Anhui University, Hefei 230601, People's Republic of China
[b] School of Life Sciences, University of Science and Technology of China, Hefei 230026, People's Republic of China

ARTICLE INFO

ABSTRACT

Ap$_4$A hydrolase (asymmetrical diadenosine tetraphosphate hydrolase, EC 3.6.1.17), an enzyme involved in a number of biological processes, is characterized as cleaving the polyphosphate chain at the fourth phosphate from the bound adenosine moiety. This paper presents the crystal structure of wild-type and E58A mutant human Ap$_4$A hydrolase. Similar to the canonical Nudix fold, human Ap$_4$A hydrolase shows the common $\alpha\beta\alpha$-sandwich architecture. Interestingly, two sulfate ions and one diphosphate coordinated with some conserved residues were observed in the active cleft, which affords a better understanding of a possible mode of substrate binding.

1. Introduction

The dinucleotide diadenosine tetraphosphate (Ap$_4$A) can be found in all living cells from *Archeae* to humans. It is produced enzymatically as a side product of protein synthesis catalyzed predominantly by aminoacyl-tRNA synthetases [1]. Ap$_4$A has been proposed to be an intracellular "alarmone" both in prokaryotes [2] and in eukaryotes [3]. Intracellularly it affects DNA repair [4], RNA processing, cell division [5], heat shock and oxidative stress [6,7], apoptosis [8,9] and transcriptional regulation [1]. In bacteria, Ap$_4$A levels may also play a role in invasion [10,11]. In addition, as an extracellular signaling molecule, Ap$_4$A may play an important role as a neurotransmitter in the cardiovascular system [12,13].

Ap$_4$A concentration appeared to increase after exposure of cells to various forms of metabolic stress such as heat, oxidative, nutritional, and DNA damage [7]. In addition, high intracellular levels of Ap$_4$A have been associated with reduced replication times [14]. Thus the regulation of Ap$_4$A levels must be tightly controlled.

Ap$_4$A hydrolase is responsible for metabolizing the "allarmone" nucleotide Ap$_4$A and is therefore involved in all the above biological processes. Recent evidence further implicates that the SARS-CoV 7a protein interacts with human Ap$_4$A-hydrolase and may participate in common pathways leading to cell cycle arrest and apoptosis [15]. Ap$_4$A hydrolase belongs to Nudix (nucleoside diphosphate linked to X) hydrolases, a superfamily of Mg^{2+}-dependent enzymes which catalyze the hydrolysis of nucleoside diphosphates linked to other moieties, X, and contains the conserved Nudix sequnce GX$_5$EX$_7$REUXEEXGU (where U represents a bulky aliphatic residue usually Ile, Leu or Val, and X represents any resi-

due) [16]. It is characterized as cleaving the polyphosphate chain at the fourth phosphate from the bound adenosine moiety. According to phylogenetic analysis [17], Ap$_4$A hydrolases were classified into two distinct groups, animal-archaeal type and plant-bacterial type enzymes. The latter contain loop insertions that undergo a large translation on substrate binding and exhibit substantial dynamic changes [18]. Previous studies of Ap$_4$A structures from both groups revealed that the enzyme has the $\alpha\beta\alpha$-sandwich architecture of a Nudix fold [18–20]. However, these studies suggest that important differences exist in the binding sites between animal-archaeal type and plant-bacterial type enzymes. According to the analysis of the NMR structure of human Ap$_4$A hydrolase (E58A), a proposal suggests recognition trigger is not required as the side chains of some key residues are on average predisposed with the correct orientation to unite key interactions for binding [19].

In this paper, we present the crystal structure of wild-type human Ap$_4$A hydrolase and its E58A mutant with/without DPO. The first structure was determined by molecular replacement at 2.7 Å resolution using the *Caenorhabditis elegans* Ap$_4$A Hydrolase structure as a search model. The mutant structures were all determined by molecular replacement at 2.1 Å resolution using the wild-type structure as a search model. Interestingly, two sulfate ions (in wild-type protein) and one diphosphate (in E58A mutant) coordinated with some conserved residues were observed in the active site, which may have important implications in the substrate binding mode in this class of enzymes.

2. Materials and methods

2.1. Cloning, expression and purification

The DNA coding sequence for human Ap$_4$A hydrolase (NCBI entry code P50583) was amplified by PCR from human brain cDNA li-

* Corresponding authors. Fax: +86 551 63861773.
  E-mail addresses: hhge@ahu.edu.cn (H. Ge), mkteng@ustc.edu.cn (M. Teng).
[1] These authors contributed equally.

brary (BD biosciences) using the following oligonucleotide primers containing artificial *Nde*I and *Xho*I sites (in bold): 5′-CTGTG**CATATG** GCCTTGAGAGCATGTGGCTTG-3′ and 5′-GAC**CTCGAG**GG CCTCTATG-GAGCAAAGAAAC-3′. The PCR product was digested with *Nde*I and *Xho*I and was ligated into the *Nde*I and *Xho*I sites of the bacterial expression vector pET22b (incorporating a C-terminal hexahistidine tag). The cloning junctions were confirmed by DNA sequencing. This recombinant plasmid was transformed into *Escherichia coli* strain BL21 (DE3). Cells were grown at 310 K in Luria–Bertani medium containing 100 μg/mL ampicillin and were harvested and sonicated in 20 mM Tris–HCl buffer pH 8.0 containing 150 mM NaCl. The lysate was clarified by centrifugation at 15,000 g for 30 min. The soluble fraction was applied to nickel-chelating resin (Amersham Biosciences) preequilibrated with equilibration buffer [20 mM Tris pH 8.0, 20 mM imidazole, 150 mM NaCl]. The resin was washed with wash buffer [20 mM Tris–HCl pH 8.0, 50 mM imidazole, 150 mM NaCl] and the target protein was eluted with elution buffer [20 mM Tris–HCl pH 8.0, 200 mM imidazole, 150 mM NaCl].

The eluate was exchanged to low-salt non-imidazole buffer (20 mM Tris pH 8.0, 20 mM NaCl) and was further purified by chromatography on a MonoQ anion ion-exchange column (GE Healthcare). The target protein was eluted using a linear gradient of 20–800 mM NaCl in 20 mM Tris pH 8.0, and then was applied to a gel filtration column (16/60 Superdex 200, GE Healthcare) in 20 mM Tris–HCl buffer pH 8.0 containing 150 mM NaCl. The flow-through fraction, which contained the target protein, was buffer exchanged with crystallization buffer (20 mM Tris–HCl pH 8.0, 20 mM NaCl, 5 mM DTT) and concentrated for crystallization assays to 10 mg/mL by centrifugal ultrafiltration (Millipore). The protein concentration was determined by Bradford method (Bio-Rad Protein Assay), using bovine serum albumin as standard. The presence and purity of the recombinant protein was then analyzed on SDS–PAGE (better than 95% purity) and was judged to be suitable for crystallization.

The E58A mutant was constructed by replacing the GAG codon for Glu58 with GCG. The construct was transformed into *E. coli* strain BL21 (DE3). The expression and purification protocols are the same as for the wild-type protein described earlier, except using the equilibration buffer instead of the wash buffer to wash the resin due to the lower affinity between the mutant protein and nickel-chelating resin.

2.2. Crystallization and data collection

The wild-type enzyme was crystallized in substrate-free form. Initial crystallization trials were set up with Crystal Screen I and Crystal Screen II reagent kits (Hampton Research) at 283 K by using the hanging-drop vapor-diffusion method. The best crystals were produced by mixing 2.0 μL of protein solution and an equal volume of reservoir solution containing 0.1 M Sodium citrate (pH 5.6), 1.2 M Lithium sulfate, 0.2 M ammonium sulfate and incubated at 277 K.

The crystals were harvested using cryoloops and immersed briefly in a cryoprotectant solution consisting of reservoir solution with the glycerol concentration raised to 15%. The crystals were subsequently flash-frozen and stored in liquid nitrogen and transferred to beamline 3W1A of the BSRF (Beijing Synchrotron Radiation Facility) for X-ray diffraction analysis and data collection.

After screening for diffraction quality, a complete data set to 2.7 Å resolution was collected using a single crystal maintained at 100 K at a wavelength of 1.0000 Å, using 1° oscillations and an exposure time of 8 s per image. The diffraction data were processed with HKL2000 program [21].

The wild-type human Ap$_4$A hydrolase crystal belongs to space group P4$_3$ with unit cell parameters $a = b = 72.49$, $c = 133.49$. Assuming the presence of four 17 kDa molecules in the asymmetric unit, a Matthews coefficient of 2.58 Å^3 Da^{-1} and a solvent content of 52.33% were calculated [22].

The E58A mutant crystals were grown by mixing the protein solution with a reservoir solution containing 0.1 M Tris (pH 8.4), 2.0 M Ammonium phosphate monobasic, 5 mM magnesium chloride and incubated at 285 K. Data were collected from crystals soaked in mother liquor with 15% glycerol added prior to flash-cooling in a liquid nitrogen stream at 100 K. A diffraction dataset of the E58A mutant crystal to 2.1 Å was collected at beamline BL17U of the SSRF (Shanghai Synchrotron Radiation Facility) at a wavelength of 1.00584 Å using 1° oscillations with a crystal-to-detector distance of 250 mm and an exposure time of 1 s per image. The diffraction data were processed with *iMOSFLM* [23] and scaled with *SCALA* from the CCP4 program suite [24].

E58A-DPO crystals were obtained by soaking E58A mutant crystals with 10 mM AP4A and 5 mM magnesium chloride. Data were collected as detailed above for the E58A mutant crystal except at a wavelength of 0.97915 Å. The diffraction data were processed with the HKL2000 program [21].

Both mutant crystals belong to space group P4$_3$2$_1$2 with two molecules in the asymmetric unit and with unit cell dimensions: E58A, $a = b = 72.19$, and $c = 133.51$; E58A-DPO, $a = b = 72.37$, and $c = 133.38$, with V$_M$ = 2.5 Å^3 Da^{-1} solvent content of approximately 51% (v/v) [22]. All crystal parameters and data collection statistics are summarized in Table 1.

2.3. Structure determination and refinement

Structure determination of the wild-type enzyme by molecular replacement was implemented with Phaser [25]. The *C. elegans* Ap$_4$A Hydrolase structure (PDB accession code 1KT9 [26]), which had 48% identity to the target structure, was used as the search model. The program Arp-Warp was then used to build from the molecular replacement model in an automated fashion. The model was completed with iterative rounds of manual building in COOT [27] and refinement in REFMAC [28]. The final refined model contains four human Ap$_4$A hydrolase molecules in the asymmetric unit and was refined to an *R* factor (*R*$_{free}$) of 21.7% (28.4%). The final model contains 432 residues, 148 water molecules, 18 sulfate ions and one glycerol. The three N-terminal residues and the last 8 C-terminal amino acids (belong to the recombinant 6×His tag) were not observed in the electron-density map.

Both mutant structures were solved by molecular replacement (MR) using the refined wild-type enzyme structure as a search model. The final E58A model has an *R* factor of 18.9% and an *R*$_{free}$ of 23.5%, while the final E58A-DPO model was refined to an *R* factor (*R*$_{free}$) of 19.1% (23.2%). Some regions (including residues 19–21 on chain B, several N- and C-terminal residues) were not modeled because of the poor electron density.

All final crystallographic models were evaluated using MolProbity [29] with all parameters within the expected value range at the resolutions. The refinement statistics are summarized in Table 1. The coordinates and structure factors have been deposited in the Protein Data Bank under the accession code 3U53, 4ICK and 4IJX.

2.4. Sequence analysis and structural presentation

Amino-acid sequences were aligned using MultAlin [30] and the structure-based sequence-alignment figure was generated using ESPript [31]. All illustrations were prepared with PyMOL [32].

Table 1
Data collection and refinement statistics.

	Wild-type	E58A	E58A-DPO
Wavelength (Å)	1.0000	1.00584	0.97915
Space group	$P4_3$	$P4_32_12$	$P4_32_12$
Molecules in ASU	4	2	2
Cell parameters *a/b/c* (Å)	72.49/72.49/133.49	72.19/72.19/133.51	72.37/72.37/133.38
Resolution range(out shell) (Å)	50–2.7 (2.775–2.705)	20–2.1 (2.154–2.10)	30–2.1 (2.157–2.103)
No. of unique reflections	17881	21385	20214
Corresponding % solvent	52.33	50.71	50.9
Rmerg[a] (out shell) (%)	9.83 (37.56)	12.7 (42.9)	8.8 (44.3)
$I/\sigma(I)$	8.5 (2.5)	15.7 (6.3)	26 (5.8)
Redundancy	7.7	13.7	13.4
Completeness (out shell) (%)	100 (100)	100 (100)	99.9 (100)
Refinement summary			
R factor[b] (%)	21.7	18.9	19.1
Free R factor[c] (%)	28.4	23.5	23.2
rmsd in bond lengths (Å)	0.018	0.013	0.013
rmsd[d] in bond angles (°)	1.609	1.589	1.642
No. of protein atoms/ASU	4553	2338	2392
No. of water molecules/ASU	148	185	122
Ramachandran plot (%)			
Ramachandran favored	98.06	97.89	97.2
Ramachandran outliers	0	0	0
PDB ID code	3U53	4ICK	4IJX

[a] $R_{merge} = \sum h \sum i |l_i h \langle ln \rangle| \sum h \sum i \langle lh \rangle$, where $\langle lh \rangle$ is the mean intensity of the *i* observations of reflection *h*.

[b] $R - factor = \sum h ||F_{obs}| - |F_{calc}|| / \sum |F_{obs}|$, where $|F_{obs}|$ and $|F_{calc}|$ are the observed and calculated structure factor amplitudes, respectively. Summation includes all reflections used in the refinement.

[c] Free R factor $= \sum ||F_{obs}| - |F_{calc}|| / \sum |F_{obs}|$, evaluated for a randomly chosen subset of 5% of the diffraction data not included in the refinement.

[d] Root-mean square-deviation from ideal values.

3. Results and discussion

3.1. Overall structure (Fig. 1)

The wild-type human Ap4A hydrolase crystallized with four monomers in the asymmetric unit and there was no evidence of higher order oligomeric assemblies in the crystal lattice, which was consistent with the purification of the enzyme as a monomer by size-exclusion chromatography (data not shown). The E58A mutant crystallized with two monomers which interacted to form a dimer through crystallographic packing. However, the mutant Ap4A hydrolase also exists as a monomeric form in solution as determined by gel filtration chromatography. The structures of all monomers from the three models are structurally similar, with RMSD (root mean square deviations) ranged from 0.14 Å to 0.41 Å for main chain atoms.

Similar to the canonical Nudix fold, the human Ap4A hydrolase monomer shows the common αβα-sandwich architecture. This contains three α-helices (α1–α3), two β sheets (composed of seven β-strands β1–β7) and loops (L1–L7). The central feature is a curved four-stranded mixed β sheet spacially arranged in the order β4β1β6β5 from left to right when facing α1. This part is sandwiched between two antiparallel α-helices (α2, α3) and α1 (roughly perpendicular to α3). There is also one short 3_{10}-helix (η1) in connecting peptides between loop L5 and β5.

3.2. Nudix interactions (Fig. 2A)

The conserved Nudix sequence motif (GX₅EX₇REUXEEXGU) is located mainly on a loop-helix-loop region (residues 43–65) as found in other known homologous structures. This segment is stabilized by a network of hydrogen bonds among conserved residues. At the N-terminus of the motif, hydrogen bonds from Glu49 to Glu46 and Arg57 clamp the helix α1 to loop L4. The first residue of the Nudix motif, Gly43, is on β4 and anchored by intrasheet hydrogen bonds to Cys6 of β1. Arg57, a conserved residue in the Nudix hydrolases, is involved in salt links with Glu49 and Glu58.

Glu62, another signature residue, helps to orient Glu110 to bind a sulfate ion by making hydrogen binds to the side chain of Glu110. At the other end of the motif, Gly64 of loop L5 makes a hydrogen bond to Arg106 carbonyl O atom of loop L7. Most of the non-conserved residues of the Nudix sequence are solvent-exposed and point away from the substrate binding cleft. However Leu52 and Leu56 help to stabilize the helix α1 on the central sheet by making hydrophobic interactions with some hydrophobic amino acids from strands β1, β5 and β6. Thus the conserved Nudix motif is of vital importance to maintaining the overall tertiary structure as well as to the enzyme activity.

3.3. Substrate binding cleft

Based on the analysis of other Ap₄A hydrolases of known structure [18–20], the potential substrate binding pocket of human Ap₄A hydrolase is a large cleft constructed by residues from β2, β3, β4, β5, β6, α1, α3, and several loops (L2, L3, L7). Two conserved aromatic residues (Tyr82, Phe128) lie at the top of the active site cleft. They play a major role in substrate binding as described previously [19,26].

The side chain of Tyr82 is well defined and its orientation would be correct for π-stacking interactions of the substrate adenine ring. However, benzene ring of Phe128 is roughly perpendicular to the phenol ring of Tyr82 based on the density for the side chain of Phe128 (although the density in monomer A and B is not as well defined as that in monomer C and D). In the E58A-DPO structure from the mutant protein crystal soaked with AP4A, which Phe128 benzene ring shows high conformational flexibility. Side chain rotation of Phe128 is therefore essential for localization of an adenine ring on the protein. Consequently, the crystal structure of the active enzyme indicates that conformational change of some important side chains would be initiated during substrate-binding step. Our proposal supports the "trigger" event proposed previously based on the X-ray structure of *C. elegans* Ap₄A hydrolase [26], another animal-archaeal type enzyme.
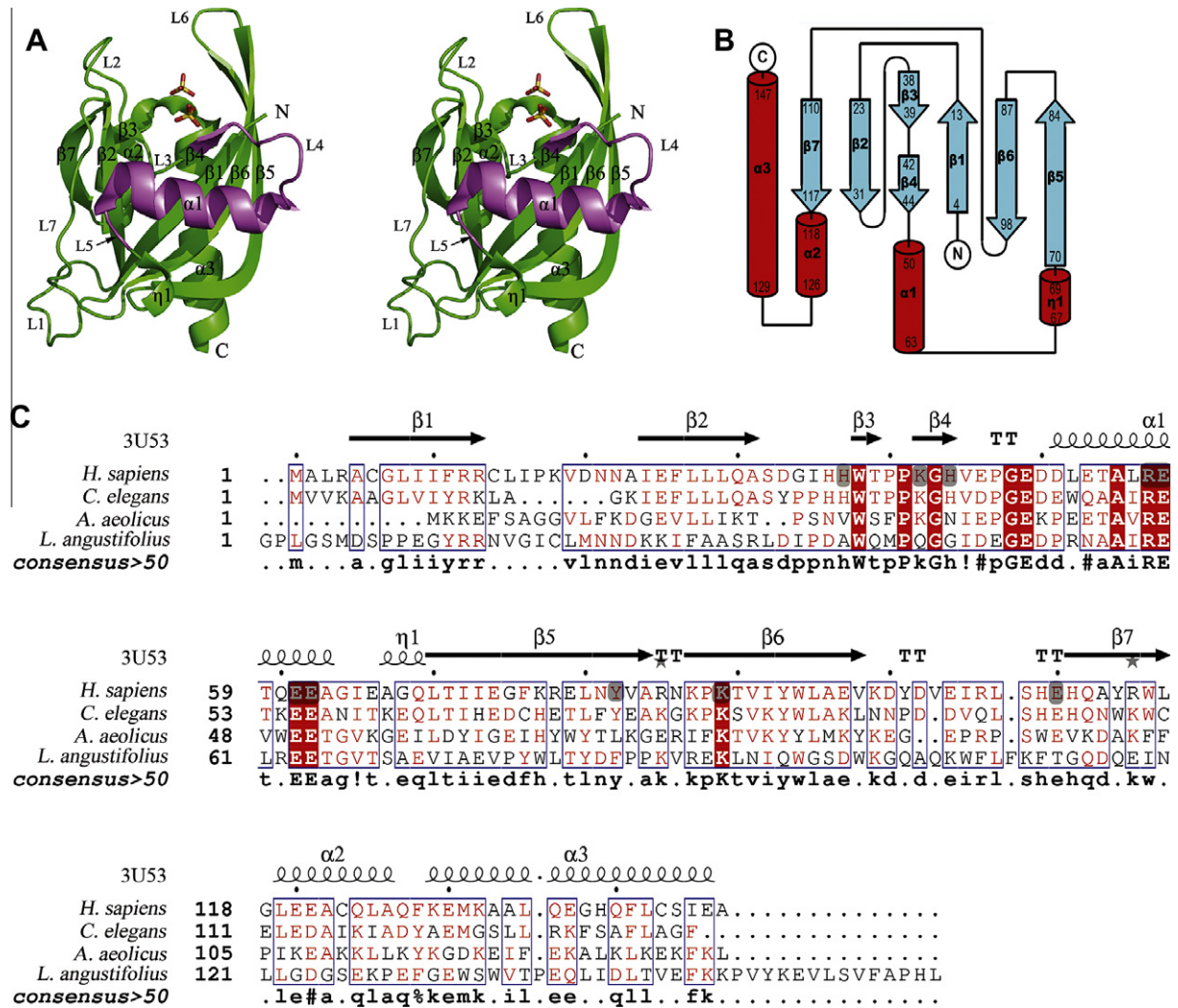
Fig. 1. (A) Stereo cartoon of human Ap4A hydrolase structure. The Nudix box is highlighted in violet. Sulfate ions are shown as sick models. (B) Topological diagram of human Ap$_4$A hydrolase with the secondary structure elements indicated. Helices and strands are shown as bars and arrows, respectively. Topology diagrams were generated with Topdraw [33]. (C) Structure-based sequence alignment of Ap$_4$A hydrolases from *Homo sapiens* (PDB code 3u53; present study), *C. elegans* (PDB code 1ktg) [26], *Lupinus angustifolius* (PDB code 1jkn) (Fletcher, Swarbrick et al. 2002) and *Aquifex aeolicus* (PDB code 3i7u) (Jeyakanthan, Kanaujia et al. 2010). Amino-acid residues which may be involved in α- and δ-phosphate interactions are in the shadow. α-helices, β-strands, and 3$_{10}$-helices are denoted by Greek characters, α, β, and η respectively. Strictly conserved residues are highlighted with red boxes. (For interpretation of the references to color in this figure legend, the reader is referred to the web version of this article.)

Examination of the electron density map for the E58A-DPO structure revealed a density feature in the active cleft of Chain B. Although there was no interpretable density for the entire AP4A molecule, the density for two phosphate groups are clearly identifiable.

3.4. The sulfate- and diphosphate- binding sites in active cleft

In the crystal structure of the wild-type human Ap$_4$A hydrolase, each monomer has one sulfate ion near the top of the substrate-binding pocket. The sulfate forms direct interactions with the protein via hydrogen bonds to His37 NE2, Lys42 NZ and Tyr82 OH (Fig. 2B). In addition, it has one oxygen atom at a distance of about 3.9 Å from the positively charged residue Lys89 NZ. In the E58A-DPO structure, one phosphate group of DPO was observed in the relevant position in Chain B, and forms the similar binding mode with the protein, while the other phosphate group, which may be the β-phosphate of the substrate, makes hydrogen binds to Lys42 NZ. (Fig. 2C).

According to the analysis of related Ap$_4$A hydrolase-substrate complexes [18–20], the analogous positions for these residues are conserved and coordinate the α-phosphate of the substrate. Hence, His37, Lys42, Tyr82 and Lys89 probably facilitate α-phosphate group binding of the real substrate. The observation of the Lys42 also suggests it could stabilize the α-phosphate as well as the β-phosphate of the substrate.

One of the monomers (chain B) in the wild-type enzyme has another sulfate ion near the Nudix sequence motif in the substrate-binding pocket, where its oxygen atoms are at hydrogen-bonding distance from the side chain ND1 and the main-chain amide of His44, OE2 of Glu110, OE1 and OE2 of Glu58. In monomer A, the equivalent position is most likely a sulfate although a water molecule was modeled in the density. In contrast, there is no relevant density in this region in monomers C and D, and the residues His44 and Glu110 show a different conformation compared to that in monomers A and B. In addition, inspection of the active site shows there is sufficient flexibility in the location of β- and γ-phosphates between the two sulfate ions sites. Thus, this sulfate position is most likely close to the substrate δ-phosphate binding site. Consequently, the sulfate is at a distance of about 3.8~5 Å from some other Nudix signature sequence residues Arg57, Clu61 and Glu62. Probably due to the lack of magnesium ions, this sulfate
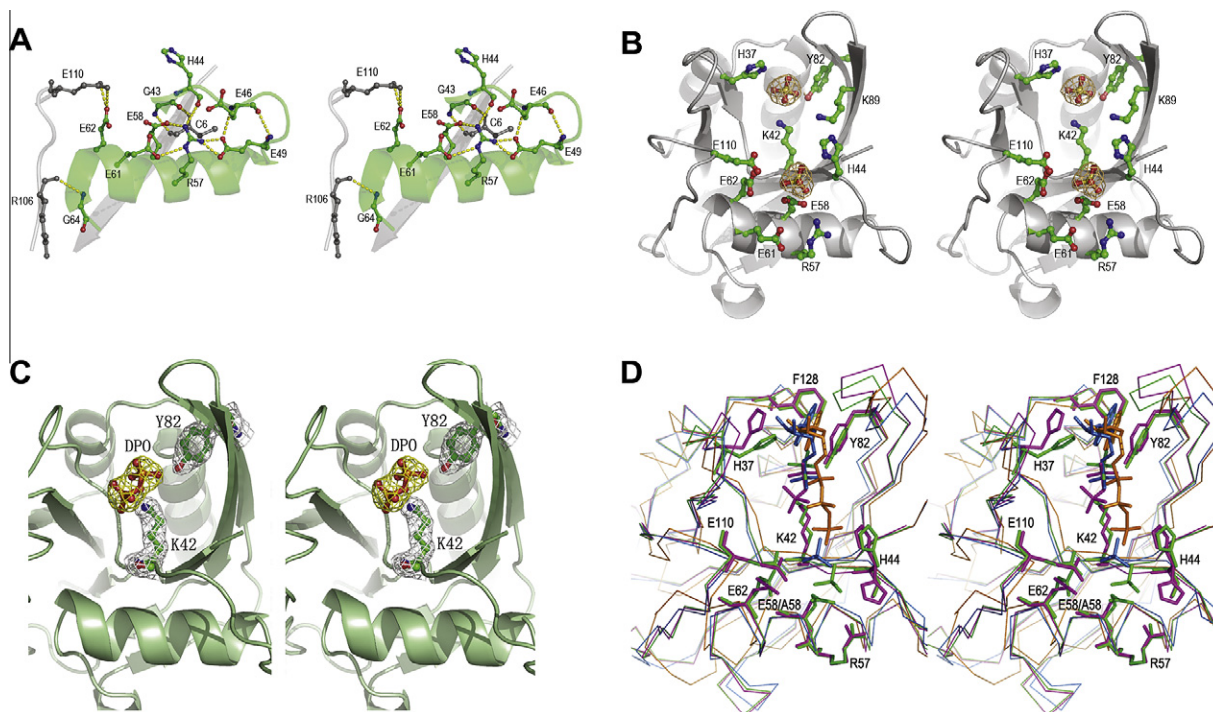
Fig. 2. (A) Hydrogen-bonding pattern of the signature sequence nudix residues of human Ap$_4$A hydrolase. The conserved residues on Nudix motif are colored. Hydrogen bonds are shown as yellow dashed lines. Close-up view of hydrogen-bond interactions of (B) sulfate ions, and (C) diphosphate in the substrate binding cleft. Electron density maps shown are F$_0$–F$_c$ simulated annealing omit maps contoured at 1δ. (D) Superposition of ribbon representation of four crystal structures of Ap4A hydrolase from *H. Sapiens* (wild-type: green, E58A-DPO: magenta), the *C. Elegans* enzyme in complex with AMP(1ktg: marine) and the *A. Aeolicus* enzyme in complex with ATP (3i7v: yellow). Residues involved in binding sulfate ions and diphosphate are shown as stick. (For interpretation of the references to color in this figure legend, the reader is referred to the web version of this article.)

position is closer to the Nudix sequence motif than the proposed δ-phosphate binding site in the crystal structure of *C. elegans* counterpart (Fig. 2D). This observation of the sulfate would suggest these residues (His44, Arg57, Glu58, Clu61, Glu62 and Glu110) are sufficient to stabilize the substrate and orientate the δ-phosphate by hydrogen bond or *via* metal coordination for nuclophilic attack.

Acknowledgments

References

[1] I. Carmi-Levy, N. Yannay-Cohen, G. Kay, E. Razin, H. Nechushtan, Diadenosine tetraphosphate hydrolase is part of the transcriptional regulation network in immunologically activated mast cells, Mol. Cell Biol. 28 (2008) 5777–5784.

[2] P.C. Lee, B.R. Bochner, B.N. Ames, ApppppA, heat-shock stress, and cell oxidation, Proc. Natl. Acad. Sci. USA 80 (1983) 7496–7500.

[3] A. Varshavsky, Diadenosine 5′, 5′′′-P1, P4-tetraphosphate: a pleiotropically acting alarmone?, Cell 34 (1983) 711–712

[4] A.G. McLennan, Dinucleoside polyphosphates-friend or foe?, Pharmacol Ther. 87 (2000) 73–89.

[5] A. Nishimura, The timing of cell division: Ap4A as a signal, Trends Biochem. Sci. 23 (1998) 157–159.

[6] M.D. Baxi, J.K. Vishwanatha, Diadenosine polyphosphates: their biological and pharmacological significance, J. Pharmacol. Toxicol. Methods 33 (1995) 121–128.

[7] L.L. Kisselev, J. Justesen, A.D. Wolfson, L.Y. Frolova, Diadenosine oligophosphates (Ap(n)A), a novel class of signalling molecules?, FEBS Lett 427 (1998) 157–163.

[8] A. Vartanian, I. Prudovsky, H. Suzuki, I. Dal Pra, L. Kisselev, Opposite effects of cell differentiation and apoptosis on Ap3A/Ap4A ratio in human cell cultures, FEBS Lett. 415 (1997) 160–162.

[9] A.G. McLennan, The MutT motif family of nucleotide phosphohydrolases in man and human pathogens (review), Int. J. Mol. Med. 4 (1999) 79–89.

[10] J.L. Badger, C.A. Wass, K.S. Kim, Identification of Escherichia coli K1 genes contributing to human brain microvascular endothelial cell invasion by differential fluorescence induction, Mol. Microbiol. 36 (2000) 174–182.

[11] T.M. Ismail, C.A. Hart, A.G. McLennan, Regulation of dinucleoside polyphosphate pools by the YgdP and ApaH hydrolases is essential for the ability of Salmonella enterica serovar typhimurium to invade cultured mammalian cells, J. Biol. Chem. 278 (2003) 32602–32607.

[12] J. Pintor, M. Diaz-Hernandez, J. Gualix, R. Gomez-Villafuertes, F. Hernando, M.T. Miras-Portugal, Diadenosine polyphosphate receptors. from rat and guinea-pig brain to human nervous system, Pharmacol. Ther. 87 (2000) 103–115.

[13] B.M. Stavrou, Diadenosine polyphosphates: postulated mechanisms mediating the cardiac effects, Curr. Med. Chem. Cardiovasc. Hematol. Agents 1 (2003) 151–169.

[14] E. Rapaport, P.C. Zamecnik, Presence of diadenosine 5′,5′′′-P1, P4-tetraphosphate (Ap4A) in mamalian cells in levels varying widely with proliferative activity of the tissue: a possible positive "pleiotypic activator", Proc. Natl. Acad. Sci. USA 73 (1976) 3984–3988.

[15] N. Vasilenko, I. Moshynskyy, A. Zakhartchouk, SARS coronavirus protein 7a interacts with human Ap4A-hydrolase, Virol. J. 7 (2010) 31.

[16] W. Xu, C.A. Dunn, C.R. Jones, G. D'Souza, M.J. Bessman, The 26 Nudix hydrolases of bacillus cereus, a close relative of bacillus anthracis, J. Biol. Chem. 279 (2004) 24861–24865.

[17] H.M. Abdelghany, L. Gasmi, J.L. Cartwright, S. Bailey, J.B. Rafferty, A.G. McLennan, Cloning, characterisation and crystallisation of a diadenosine 5′,5′′′-P(1), P(4)-tetraphosphate pyrophosphohydrolase from Caenorhabditis elegans, Biochim. Biophys. Acta 1550 (2001) 27–36.

[18] J.I. Fletcher, J.D. Swarbrick, D. Maksel, K.R. Gayler, P.R. Gooley, The structure of Ap(4)A hydrolase complexed with ATP-MgF(x) reveals the basis of substrate binding, Structure 10 (2002) 205–213.

[19] J.D. Swarbrick, S. Buyya, D. Gunawardana, K.R. Gayler, A.G. McLennan, P.R. Gooley, Structure and substrate-binding mechanism of human Ap4A hydrolase, J. Biol. Chem. 280 (2005) 8471–8481.

[20] J. Jeyakanthan, S.P. Kanaujia, Y. Nishida, N. Nakagawa, S. Praveen, A. Shinkai, S. Kuramitsu, S. Yokoyama, K. Sekar, Free and ATP-bound structures of Ap4A hydrolase from Aquifex aeolicus V5, Acta Crystallogr. D Biol. Crystallogr. 66 (2010) 116–124.

[21] Z. Otwinowski, W. Minor, Processing X-ray diffraction data collected in oscillation mode, Methods Enzymol. 276 (1997) 307–326.

[22] B.W. Matthews, Solvent content of protein crystals, J. Mol. Biol. 33 (1968) 491–497.

[23] T.G. Battye, L. Kontogiannis, O. Johnson, H.R. Powell, A.G. Leslie, IMOSFLM: a new graphical interface for diffraction-image processing with MOSFLM, Acta Crystallogr. D Biol. Crystallogr. 67 (2011) 271–281.

[24] M.D. Winn, C.C. Ballard, K.D. Cowtan, E.J. Dodson, P. Emsley, P.R. Evans, R.M. Keegan, E.B. Krissinel, A.G. Leslie, A. McCoy, S.J. McNicholas, G.N. Murshudov, N.S. Pannu, E.A. Potterton, H.R. Powell, R.J. Read, A. Vagin, K.S. Wilson, Overview of the CCP4 suite and current developments, Acta Crystallogr. D Biol. Crystallogr. 67 (2011) 235–242.

[25] A.J. McCoy, R.W. Grosse-Kunstleve, P.D. Adams, M.D. Winn, L.C. Storoni, R.J. Read, Phaser crystallographic software, J. Appl. Crystallogr. 40 (2007) 658–674.

[26] S. Bailey, S.E. Sedelnikova, G.M. Blackburn, H.M. Abdelghany, P.J. Baker, A.G. McLennan, J.B. Rafferty, The crystal structure of diadenosine tetraphosphate hydrolase from Caenorhabditis elegans in free and binary complex forms, Structure 10 (2002) 589–600.

[27] P. Emsley, K. Cowtan, Coot: model-building tools for molecular graphics, Acta Crystallogr. D Biol. Crystallogr. 60 (2004) 2126–2132.

[28] G.N. Murshudov, A.A. Vagin, E.J. Dodson, Refinement of macromolecular structures by the maximum-likelihood method, Acta Crystallogr. D Biol. Crystallogr. 53 (1997) 240–255.

[29] S.C. Lovell, I.W. Davis, W.B. Arendall 3rd, P.I. de Bakker, J.M. Word, M.G. Prisant, J.S. Richardson, D.C. Richardson, Structure validation by Calpha geometry: phi, psi and Cbeta deviation, Proteins 50 (2003) 437–450.

[30] F. Corpet, Multiple sequence alignment with hierarchical clustering, Nucleic Acids Res. 16 (1988) 10881–10890.

[31] P. Gouet, E. Courcelle, D.I. Stuart, F. Metoz, ESPript: analysis of multiple sequence alignments in postscript, Bioinformatics 15 (1999) 305–308.

[32] W.L. DeLano, The PyMOL Molecular Graphics System, DeLano Scientific, Palo Alto, CA, USA, 2002.

[33] C.S. Bond, Topdraw: a sketchpad for protein structure topology cartoons, Bioinformatics 19 (2003) 311–312.